Mater. Res. Soc. Symp. Proc. Vol. 1805 © 2015 Materials Research Society
DOI: 10.1557/opl.2015.687

Thermoelectric Properties of ZnO Thin Films Grown by Metal-Organic Chemical Vapor Deposition

Bahadir Kucukgok[1], Babar Hussain[1], Chuanle Zhou[1], Ian T. Ferguson[2], and Na Lu[3]

[1]Department of Electrical and Computer Engineering, University of North Carolina at Charlotte, 9201 University City Blvd, Charlotte, NC 28223, U.S.A
[2]College of Engineering and Computing, Missouri University of Science and Technology, 305 McNutt Hall, 1400 N. Bishop, Rolla, MO 65409, U.S.A
[3]Department of Engineering Technology, University of North Carolina at Charlotte, 9201 University City Blvd, Charlotte, NC 28223, U.S.A

ABSTRACT

Thermoelectric (TE) materials have gained renewed interests in last decades for both power generation and energy conservation from waste-heat harvesting. Research in the discovery of best TE materials such as, bulk materials, complex structures, and low dimensional play crucial role to achieve high efficiency TE materials. Wide bandgap materials like ZnO can be promising candidate for high efficiency TE power generation owing to its low-cost, nontoxicity, and stability at high temperatures. In this paper, room temperature TE properties of thin film ZnO grown by metal organic vapor deposition (MOCVD) are reported. TE properties of thin film GaN are also studied as reference to that of thin film ZnO. Moreover, high resolution x-ray diffraction (HRXRD), room temperature photoluminescence (PL) with deep ultraviolet (DUV) spectroscopy (excitation at 248nm), hall effect, and thermal gradient methods have been employed to investigate the effect of structural, optical, electrical, and thermal properties of the samples, respectively. The effect of doping concentrations and structural defects on Seebeck coefficients of thin film ZnO are systematically studied and discussed in this work.

INTRODUCTION

Due to growing demand on cost-effective and renewable energy sources, converting electricity directly from waste heat sources by using thermoelectric (TE) devices has attracted extensive interest in the field of energy generation [1-5]. Although high efficiency TE devices have shown promising properties, their applications are limited compare to other forms of small scale power generation sources due to their low energy conversion efficiencies [4,6,7]. Therefore TE materials have been studied extensively over the last two decades to improve its efficiency [3]. The efficiency of the TE materials is determined by dimensionless TE figure of merit, defined as $ZT=(S^2\sigma)/(\kappa_e+\kappa_l)$, where S is the Seebeck coefficient, σ is the electrical conductivity, T is the temperature, κ_e is the electrical thermal conductivity, and κ_l is the lattice thermal conductivity. Thus, minimizing the thermal conductivity and, at the same time, maximizing the power factor ($S^2\sigma$) are required in order to achieve good TE performance [8-10]. However, there is a strong interrelation between power factor and thermal conductivity. For instance, via Wiedemann–Franz relation, which is defined as $\kappa_e=L\sigma T$, where L is the Lorentz number, electrical conductivity (σ) and electrical thermal conductivity (κ_e) are dependent variables and vary simultaneously [1,7,9,10]. Thus, these drawbacks often result in main hindrance for obtaining $ZT\geq1$. Up until know, various experimental efforts have been conducted to improve

TE properties, particularly for reducing the lattice thermal conductivity. Most effective mechanisms of optimizing the thermal conductivity are nanostructuring and alloying [2,5]. For instance, increasing the phonon scattering at boundaries and interfaces [10] via nanostructuring can reduce lattice thermal conductivity without too much deteriorating the electrical conductivity. Additionally, disordering the crystal structure via introducing host atoms in the matrix through alloying, which creates scattering centers and mass fluctuations, reduces the thermal conductivity of materials [3].

BiTe, PbTe, AgPbSbTe nanostructured alloys, layered zintl phases $Yb_{14}MnSb_{11}$, and SiGe have been recognized as the promising TE materials at room temperature and high temperatures [8,11,12]. However, the use of those materials is limited due to their high-cost, scarcity of availability, toxicity, and production difficulties. Therefore, oxide-based materials, as alternative TE candidates have drawn great interest on TE research because of their cost-effectiveness, excellent durability, non-toxicity, elemental abundance, and thermal stability at high temperatures. In particular, ZnO-based materials are attractive candidates for high temperature TE applications due to their remarkable TE performance among other semiconductor oxides. For instance, Ga and Al dual-doped ZnO is the best reported n-type oxide TE materials [13]. Unlike commercially available TE materials, ZnO has noncomplex wurtzite structure, low effective mass ($0.24m_e$), and high thermal conductivity ($40 Wm^{-1}K^{-1}$ for bulk ZnO at 300K), which prevents it from obtaining high *ZT* values [7,11]. However, improving electrical properties (i.e., both high Seebeck coefficient and electrical conductivity) result in enhance *ZT* values [1, 9]. For instance, carrier density refinement by Al and Ga doping exhibits *ZT*=0.65 at 1247K and 0.5 at. % indium doping results in *ZT*=0.45 at 1000K in ZnO [11]. Additionally, one of the most well-known n-type oxide TE materials, $SrTiO_3$, has a highest *ZT* value of 0.37 [14]. $Ca_3Co_4O_9$ and Na_xCoO_2 as a p-type oxide semiconductors reveal promising *ZT* values of 0.61 [15] and 0.92 [16], respectively. Moreover, it has been lately observed that, two-dimensional electron gas (2DEG) ZnO shows very high mobility ($>300.000 cm^2V^{-1}s^{-1}$) due to the charge accumulation at the interface, thereby it becomes essential for TE applications [17]. Furthermore, zinc oxide (ZnO) as a wide band gap semiconductor is an inherently n-type semiconductor and has been utilized for variety of applications such as, solar cells, gas sensors, piezoelectric transducers, light-emitting diodes, and recently TE devices.

In this study, electrical and thermal properties of unintentionally doped ZnO thin films grown by MOCVD are examined to understand the TE performance and the optimized carrier densities. TE properties of thin film GaN samples are also studied as reference to that of thin film ZnO. The effect of structural and optical properties on Seebeck coefficients of thin film ZnO are systematically studied and discussed.

EXPERIMENT

The samples studied here include thin film ZnO and thin film GaN. Unintentionally doped ZnO thin film samples were grown on c-axis 2 in. sapphire wafer by metal organic vapor deposition method (MOCVD) and Zn face of (0001) bulk ZnO samples were provided from Cermet Inc. Thin film GaN samples with various doping concentrations were also grown on c-axis 2 in. sapphire wafer by MOCVD. The standard in-plane Seebeck measurement is performed in this study. Details of the theory and experiments setup were discussed in elsewhere [9]. The electrical characterizations were performed by hall effect measurement methods in the in-plane direction. For Seebeck and hall measurements, Ti/Al/Ti/Au ohmic electrodes were deposited on

the top n-GaN layers. Moreover, high resolution x-ray diffraction (HRXRD) measurements were performed using a Philips X'Pert MRD triple-axis diffractometer equipped with a four crystals Ge (220) monochromator in the incident beam optics and a Cu sealed anode and room temperature photoluminescence (PL) analyses by utilizing deep ultraviolet (DUV) spectroscopy (excitation at 248nm), to investigate the effect of structural and optical properties of the samples, respectively.

DISCUSSION

Figures 1 (a) and (b) illustrate the electrical conductivity and mobility of unintentionally doped thin film ZnO samples, respectively. It should be noted that thin film ZnO samples are unintentionally doped that lead to an enhancement of the carrier density and consequently the electrical conductivity. It can be clearly observed that electrical conductivity and mobility increase gradually as the carrier density increases. The highest electrical conductivity $366\Omega^{-1}cm^{-1}$ and mobility $23cm^2V^{-1}s^{-1}$ are found at $9.89\times10^{19}cm^{-3}$. Additionally, the electrical conductivity and mobility exhibit a sudden increase starting at $4\times10^{19}cm^{-3}$, which could be attributed to impact of point defects, such as oxygen vacancy and/or Zn interstitial. This is because slight variation in the oxygen content results in compositional defects similar to oxygen vacancies or zinc interstitials, which act as donors and these defects results in scattering of electrons, therefore induces electrical conductivity increment or decrement. For instance, as the scattering centers increase the electrical conductivity decreases since mobility decreases at the same time as well.

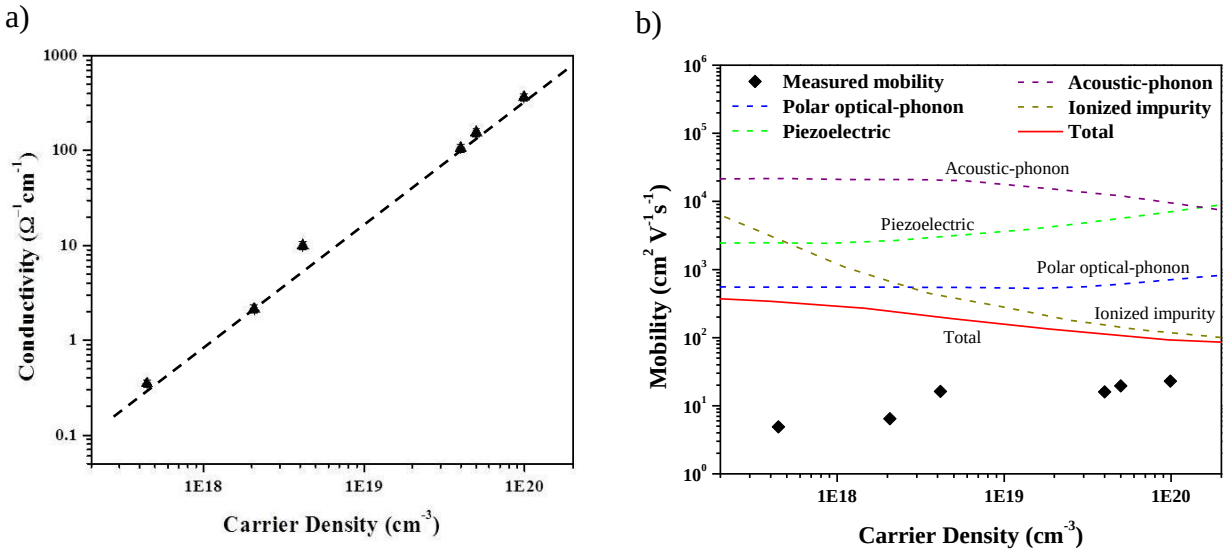

Figure 1: (a) Electrical conductivity and (b) mobility of thin film ZnO as function of carrier density at 300K (The dashed line is guided to the eye). *x* and *y* axes are logarithmic scale for both figures. In Figure 1 (b), the influences of different scattering mechanisms to the total mobility are depicted by dashed curves.

The mobility is measured between the values of 5 to $20cm^2V^{-1}s^{-1}$, which are relatively poor compared to thin film GaN at similar carrier densities, however these values are in agreement with other reported results [18,19]. The contribution of different scattering mechanisms on ZnO mobility is presented in Figure 1 (b) using the Boltzmann transport equation with a variational

method. The list of material properties to calculate the electron scattering mechanisms including polar optical-phonon scattering, ionized impurity scattering, acoustic-phonon scattering, and piezoelectric interactions are also determined in reference [20]. It can be observed that electron mobility data dramatically increases and becomes closer to the theoretical limit as the carrier density increases. However, the measured values are considerably lower than that of those calculated ones. The unexpected trend; that is, mobility increases with carrier density could be explained in terms of electron-plasmon interaction [18,20]; and it also proposes that under a certain level, scattering mechanisms don't have significant influence on mobility.

The Seebeck coefficient and power factor are important parameters characterizing the TE properties. Figures 2 (a) and (b) show the absolute Seebeck coefficient and power factor of thin film ZnO with the function of carrier density at 300K, respectively. For comparison, Seebeck values of thin film GaN at similar carrier density are also illustrated. The Seebeck values of thin film ZnO are measured between 20 to 110μV/K. The absolute value of the Seebeck coefficient is decreased by a rising amount of these defects due to an increase of the charge carrier density and highest Seebeck coefficient 110μV/K was found at carrier density 4.45×10^{17}cm^{-3}. Evidently, Seebeck values of thin film GaN are much higher than those of thin film ZnO samples. This is because interstitial defects like oxygen vacancies act as additional scattering centers and results in low crystalline quality hence lower Seebeck values in ZnO (Figures 3 and 4).

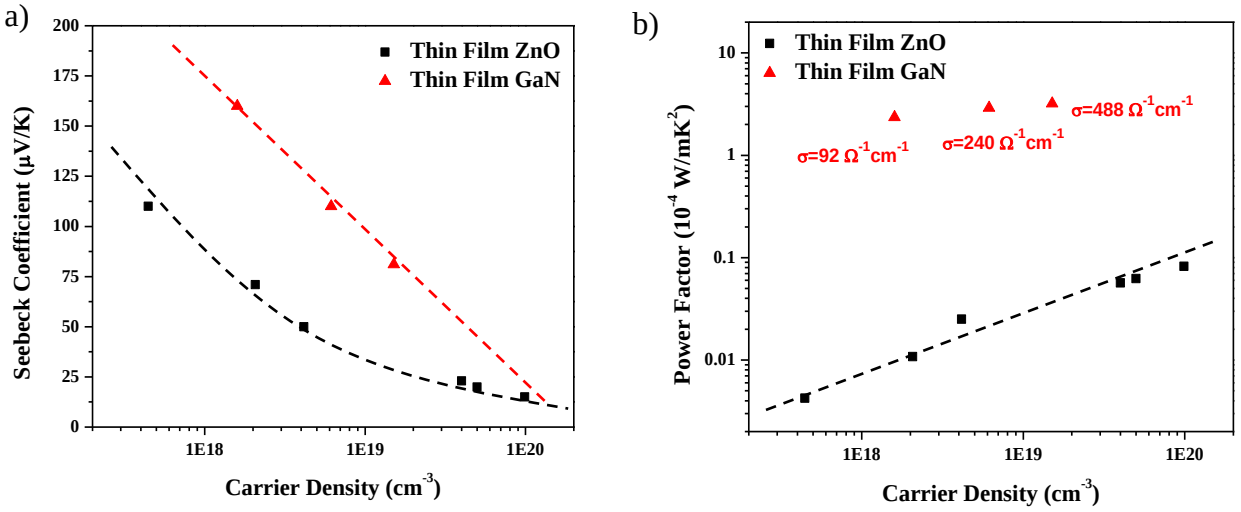

Figure 2: (a) Absolute Seebeck coefficient and (b) power factor as a function of carrier density at 300K. *x* and *y* axes are logarithmic scale in Figure 2 (b). Dashed lines are guided to the eyes.

Additionally, from HRXRD scans it was calculated that the screw and mixed dislocation density of thin film GaN is in the range of 10^{7}cm^{-2} whereas 10^{10}cm^{-2} for thin film ZnO. Thus, it can be attributed that high dislocation density leading to a corresponding decrease in the Seebeck coefficient. Furthermore, for different type of thin films various scattering mechanisms might play dominant role other than single dislocation scattering and thus result in different Seebeck coefficients at similar carrier densities. The efficiency of the TE material can be calculated by the electrical conductivity and the Seebeck coefficient (PF=$S^2\sigma$). As seen in Figure 2 (b) power factor increases gradually with carrier density. The highest power factor 0.083×10^{-4}W/mK^2 was found at carrier density 9.89×10^{19}cm^{-3}. The power factors of thin GaN samples are far above from ZnO samples at similar carrier densities due to their high electrical conductivity values.

Figure 3 (a) depicts the PL spectrum of thin films ZnO samples. The spectra show near bad-edge emission peaks slightly varies between 3.26eV and 3.31eV. Insets show deep level emission (DLE) which can be attributed to intrinsic defects, such as zinc vacancy V_{Zn}, oxygen vacancy V_O, interstitial zinc Z_{ni}, and antisite oxygen O_{Zn}. Additionally, from the whole spectrum it can be clearly observed that these defects centers contributed to the bandgap of the material and result in larger full-width at half-maximum (FWHM) values. Lower Seebeck coefficient related to degenerate film quality can also be evaluated from PL spectrums in which as FWHM increases Seebeck coefficient decreases.

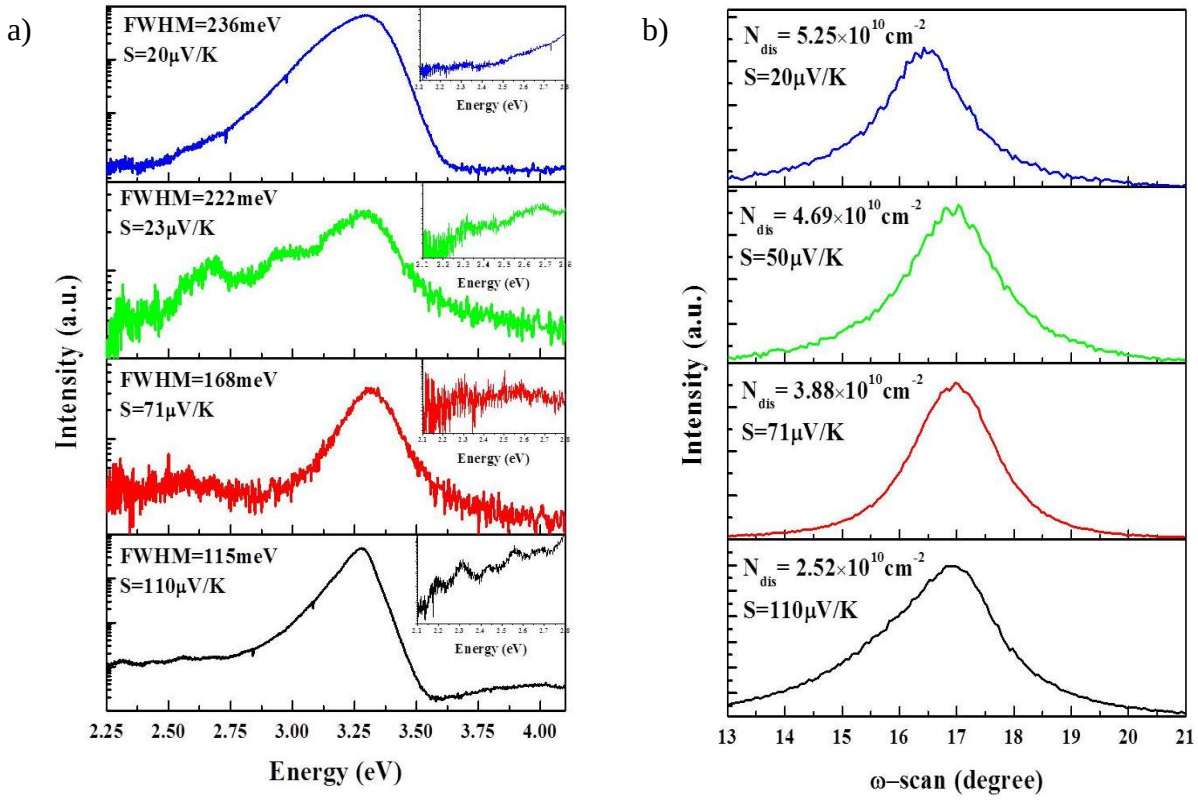

Figure 3: (a) PL analyses of thin film ZnO by utilizing deep DUV spectroscopy (excitation at 248nm) at 300K. Insets show the deep level emissions. FWHM and Seebeck values of each spectrum are also shown (b) rocking curve HRXRD scans on thin film ZnO at 300K. Screw and mixed dislocation and Seebeck values are also shown.

Rocking curve HRXRD analyses of thin film ZnO samples are shown in Figure 3 (b) and impact of screw and mixed dislocation density on Seebeck coefficients are evaluated. It is known that dislocations play a role in limiting electron transport in thin films particularly at high densities ($\geq 10^{10}$cm^{-2}) and found in the range of 10^{10}cm^{-2} for thin film ZnO, which can be assumed as high dislocation density films. It can be realized that Seebeck coefficient decreases while increasing dislocation density. This might be attributed to decreasing the value of relaxation time with increasing dislocation density and result in variance in the Seebeck coefficient due to its stronger dependence of the relaxation rates on energy.

CONCLUSIONS

The electrical and thermal properties of unintentionally doped thin film ZnO materials are investigated. TE results of thin film GaN is integrated to thin film ZnO to make comparison. The structural and optical properties are evaluated in order to correlate and understand the impact of defects on TE properties. It was found that Seebeck coefficient is much higher than that of thin film ZnO at similar carrier densities, which could be attributed to impact of scattering centers particularly dislocation scattering.

REFERENCES

1. N. Lu and I. Ferguson, *Semicond. Sci. Technol.* **28**, 074023 (2013).
2. Y. Saeed, N. Singh, and U. Schwingenschlogl, *Appl. Phys. Lett.* **104**, 033105 (2014).
3. M. W. Gaultois, and T. D. Sparks, *Appl. Phys. Lett.* **104**, 113906 (2014).
4. B. Wang, B. Kucukgok, Q. Hea, A. G. Melton, J. Leacha, K. Udwarya, K. Evans, N. Lu and I. T. Ferguson, *MRS Online Proceedings Library*, **1558** (2013).
5. H. Zhu, W. Sun, R. Armiento, P. Lazic, and G. Ceder, *Appl. Phys. Lett.* **104**, 082107 (2014).
6. M. H. Elsheikh, D. A. Shnawah, M. F. M. Sabri, S. B. M. Said, M. H. Hassan, M. B. A. Bashir, M. Mohamad, *Renewable and Sustainable Energy Reviews* **30**, 337–355 (2014).
7. P. Jood, R. J. Mehta, Y. Zhang, T. Borca-Tasciuc, S. X. Dou, D. J. Singh and G. Ramanath, *RSC Adv.* **4**, 6363 (2014).
8. D. Gautam, M. Engenhorst, C. Schilling, G. Schierning, R. Schmechel, and M. Winterer, *J. Mater. Chem. A*, **3**, 189-197 (2015).
9. B. Kucukgok, B. Wang, A. G. Melton, N. Lu, and I. T. Ferguson, *Phys. Status Solidi C*, **11,** 894–897 (2014).
10. L. Brockway, V. Vasiraju, M. K. Sunkara, and S. Vaddiraju, *ACS Appl. Mater. Interfaces*, **6**, 14923−14930 (2014).
11. S. Saini , P. Mele, H. Honda, D. J. Henry, P. E. Hopkins, L. Molina-Luna, K. Matsumoto, K. Miyazaki, and A. Ichinose, *Jpn. J. Appl. Phys.* **53**, 060306 (2014).
12. H. Alama, S. Ramakrishna, *Nano Energy*, **2**, 190–212 (2013).
13. J. C. Fan, K. M. Sreekanth. Z. Xie, SL. Chang, K.V. Rao, *Progress in Materials Science*, **58**, 874-985 (2013).
14. A. Kikuchi, N. Okinaka, T. Akiyama, *Scr. Mater.* **63**, 407−410 (2010).
15. N. V. Nong, N. Pryds, S. Linderoth, M. Ohtaki, *Adv. Mater.* **23**, 2484−2490 (2011).
16. M. Ito, D. Furumoto, *J. Alloys Compd.* **450**, 517− 520 (2008).
17. R. Takayanagi, T. Fujii, and A. Asamitsu, *Jpn. J. Appl. Phys.* **53**, 111101 (2014).
18. T. Makino, Y. Segawa, A. Tsukazaki, A. Ohtomo, and M. Kawasaki, *Appl. Phys. Lett.* **87** (2005).
19. A. Tsukazaki, A. Ohtomo, and M. Kawasaki, *Appl. Phys. Lett.* **88** (2006).
20. M. V. Fischetti, *Phys Rev B.* **44**, 5527 (1991).